Influence of Pulse Shaping on Bit Error Rate Performance and Out of Band Radiation of Generalized Frequency Division Multiplexing

Maximilian Matthé, Nicola Michailow, Ivan Gaspar, Gerhard Fettweis
Vodafone Chair Mobile Communication Systems
Technische Universität Dresden, 01069 Dresden, Germany
{maximilian.matthe|nicola.michailow|ivan.gaspar|fettweis}@ifn.et.tu-dresden.de

***Abstract*—Generalized Frequency Division Multiplexing (GFDM) is a multicarrier transmission scheme that offers flexible pulse shaping of individual subcarriers. The application of pulse shaping per subcarrier can control the out of band (OOB) radiation and create non-orthogonal waveforms. In this paper, the influence of the pulse shaping to the overall system performance, namely bit error rate (BER) over AWGN channels and OOB radiation, is investigated. Closed from expressions for the BER and power spectral density (PSD) of GFDM are derived. Simulation results show that GFDM reduces the OOB radiation by 46dB compared to OFDM, while at the same time, the OFDM BER can be achieved when using the Dirichlet pulse filter. In case some self-interference is allowed, the OOB radiation can be reduced even more, which is a key aspect for cognitive radio (CR) applications.**

***Index Terms*—flexible physical layer, intercarrier interference, multicarrier modulation**

I. Introduction

Machine to machine (M2M) communication has developed to an active research area in the past years. In the future the increasing demand for smart devices and e.g. environmental monitoring systems will raise the number of wireless sensors and devices considerably. Upcoming 5th generation cellular networks (5G) need to be capable of handling this highly increased number of network participants as well as a significant growth in data volume. Sporadic random access from many M2M devices can be achieved with cognitive radio (CR) techniques, where flexibility in shaping and structuring the transmit signal is a key aspect. A CR system needs to be able to flexibly aggregrate spectrum white spaces where at the same time the OOB leakage is minimized in order to not affect neighboring systems.

Current cellular transmission schemes like Long-Term-Evolution (LTE) and LTE-A employ the well known orthogonal frequency division multiplexing (OFDM) in the PHY layer. Although OFDM is very robust in frequency-selective channels and offers an efficient implementation, it is not well suited for future requirements. OFDM is very sensitive to carrier frequency offsets and requires a very fine synchronization. Its large OOB leakage makes it unattractive for CR applications and the requirement for a cyclic prefix (CP) in every OFDM symbol limits its spectral efficiency. Consequently, new multicarrier transmission schemes are investigated that address these problems. Amongst them, filter bank multicarrier (FBMC) [1] and generalized frequency division multiplexing (GFDM) [2] are promising candidates for 5G applications. FBMC is a transmission scheme that employs a prototype pulse shaping filter on every subcarrier to reduce the OOB radiation and Offset-QAM is used to ensure a quasi-orthogonal transmission of the data symbols. Several literature on the filter design for FBMC has been published where the minimization of the OOB radiation under the constraint of perfect reconstruction [3] or near-perfect reconstruction [4] is investigated. GFDM is a block-based multicarrier transmission scheme that is also derived from the filter bank approach [5]. The transmit data of each block is distributed in time and frequency and each subcarrier is pulse-shaped with an adjustable filter. Tail-biting is employed to remove the need for additional guard intervals and to provide an efficient FFT-based implementation. The insertion of a cyclic prefix in each block instead in each symbol increases the spectral efficiency compared to OFDM and still offers the means for an efficient channel equalization in the frequency domain. GFDM can adapt the block dimension to a particular transmission scenario and the pulse shaping filter controls the OOB leakage and self-interference. Methods for the cancellation of the self-interference with a matched filter (MF) receiver have been proposed in [6] that show almost equal performance as orthogonal systems. A drawback of GFDM is its increased complexity when compared to OFDM. The main goal of this paper is to analyze the GFDM receiver theoretically and to provide closed form solutions for the PSD and the BER of GFDM with a matched filter receiver. Based on these equations the influence of different pulse shaping filters on the BER and OOB radiation is investigated in detail. The remainder of this paper is organized as follows: Section II shortly describes the GFDM system in the notation that will be used throughout this paper. The closed form solution for the BER is derived in Section III and a closed form expression for the PSD of GFDM is provided in Section IV. Simulation results for different pulse shaping filters are given in Section V and a final conclusion is provided in Section VI.

II. GFDM System Description

GFDM is a block-based multicarrier transmission scheme where each block contains KM complex valued data symbols

978-1-4799-4640-2/14/$31.00 ©2014 IEEE

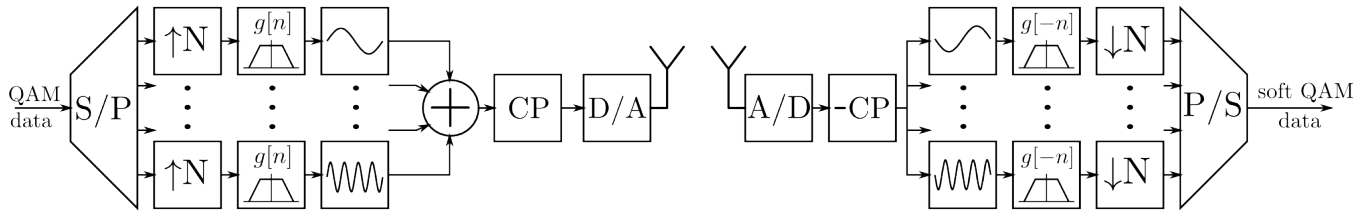

(a) Transmitter (b) Matched filter receiver

Fig. 1. Block diagram of the baseband GFDM transceiver.

that are distributed into M time and K frequency slots. The subcarriers in GFDM are spaced at $1/T_S$ and each GFDM block has a time duration of MT_S where T_S is the symbol duration. The sampling frequency is set to N/T_S resulting in N samples per symbol and MN samples per block. Consequently the sampling theorem constraints the subcarrier count to $K \leqslant N$.

GFDM employs a normalized pulse shaping filter that is circular with periodicity $n|_{NM}\,(n \mod MN)$ in order to achieve the tail-biting, i.e. circular convolution, at the transmitter.

A. GFDM Transmitter

The block diagram of the GFDM transmitter in baseband is shown in Fig. 1a. The depicted GFDM transmission operation before CP insertion can be expressed as the weighted superposition of K subcarrier signals according to

$$x[n] = \sum_{m=0}^{M-1} \sum_{k=0}^{K-1} d_{km} g_{km}[n] \quad n = 0, \ldots, MN-1, \tag{1}$$

where

$$g_{km}[n] = g[(n - mN)|_{MN}] \cdot e^{-j2\pi \frac{kn}{N}} \tag{2}$$

is a shifted version of the circular prototype filter $g[n]$, which is delayed by mN in time and $\frac{k}{N}$ in frequency. The $g_{km}[n]$ are weighted by the complex valued data symbols d_{km}, which are constrained to be i.i.d. with unit variance and are taken from a standard X-QAM alphabet, to obtain the complete transmit signal. It is already evident from (1) that a linear matrix model exists that resembles the transmit equation in a simpler manner. The detailed derivation is contained in [7] and accordingly (1) can be rewritten as

$$\vec{x} = \mathbf{A}\vec{d}, \tag{3}$$

where $\vec{x}$ is the a column vector that contains the samples of $x[n]$, $\mathbf{A}$ is the $NM \times KM$ transmitter matrix and $\vec{d}$ the vector with the complex data symbols. $\vec{d}$ and $\mathbf{A}$ contain the data symbols and the shifted prototype filters in the following order:

$$\mathbf{A} = (\vec{g}_{0,0}, \ldots, \vec{g}_{K-1,0}, \vec{g}_{0,1}, \ldots, \vec{g}_{0,M-1}, \ldots, \vec{g}_{K-1,M-1}) \tag{4}$$

$$\vec{d} = (d_{0,0}, \ldots, d_{K-1,0}, d_{0,1}, \ldots, d_{0,M-1}, \ldots, d_{K-1,M-1})^T \tag{5}$$

Here, $\vec{g}_{km}$ is the column vector containing the samples of $g_{km}[n]$.

B. Channel Model

To find closed form BER equations the transmit signal $\vec{x}$ passes an AWGN channel

$$\vec{y} = \vec{x} + \vec{n}, \tag{6}$$

where $\vec{n} \sim \mathcal{N}(0, \sigma_n^2 \mathbf{I}_{MN})$ is the AWGN vector with noise variance σ_n^2 and $\mathbf{I}_{MN}$ is the $MN \times MN$ identity matrix. Simulation results for BER performane in Rayleigh fading channels are given in [7].

C. Matched Filter GFDM Receiver

The block diagram for the matched filter GFDM receiver is shown in Fig. 1b. The matched filter receiver is employed because it has a very low complexity and minimizes the noise influence in AWGN. With sophisticated interference cancellation schemes the MF performance can be arbitrarily close to an orthogonal system, as is shown in [6]. Each subcarrier of the received signal $\vec{y}$ is filtered separately with the corresponding circular matched filter. Afterwards, each filtered subcarrier is sampled at the symbol slots to obtain the detected data symbols. According to [7] this operation is expressed in a matrix equation as

$$\hat{\vec{d}} = \mathbf{A}^{\mathrm{H}}\vec{y} = \mathbf{S}\vec{d} + \mathbf{A}^{\mathrm{H}}\vec{n} \tag{7}$$

where $\mathbf{S} = \mathbf{A}^{\mathrm{H}}\mathbf{A}$ is the $KM \times KM$ system matrix of the GFDM transceiver.

D. Pulse Shaping Filters

This section contains a summary of the circular GFDM pulse shaping filters that will be investigated in the simulation. Their time domain response is shown in Fig. 2.

1) Root Raised Cosine and Raised Cosine: The well known raised cosine and root raised cosine pulse shaping filters are designed in the time domain according to the required rolloff factor α.

2) Xia Pulse: The Xia pulses, first published in [8], are a family of real non-symmetric pulse shaping filters that are defined by a rolloff factor α and a rolloff function ν in the frequency domain. According to [9] results for the 1st and 4th order Xia pulse are given. The time domain response for both Xia pulses with rolloff $\alpha = 0.5$ is shown in Fig. 2.

3) Gaussian Pulse: The Gaussian pulse is defined in the time domain by

$$g_{\text{Gauss}}[n] = \frac{\sqrt{\pi}}{\alpha} \exp\left(-\frac{\pi^2 n}{\alpha^2 N}\right) \tag{8}$$

where α is its variance in the time domain.

4) Dirichlet Pulse: The Dirichlet pulse is defined by a perfect rect function in the frequency domain with the width of M frequency bins that are located around the DC bin, so that the time domain response is a Dirichlet kernel [10]. The Dirichlet pulse is a corner case of the Xia pulse when the rolloff goes to zero.

E. Guard Symbol Insertion

For the spectrum of the GFDM signal not only the pulse shaping but also the transition between subsequent blocks is important, since an abrupt change of the signal between two blocks creates a high OOB radiation. In order to achieve more smooth transitions, a guard symbol can be inserted into each block, which means that $d_{k0} = 0$ for all subcarriers. The corresponding reduced spectral efficiency of $\frac{M-1}{M}$ can be minimized with a high symbol count. Fig. 3 illustrates the insertion of a guard symbol.

III. Closed Form Solution for the BER of GFDM

Based on the observations in Section II-C the BER of GFDM with a matched filter receiver over an AWGN channel can be derived from the probability distribution of the self-interference.

A. Probability Distribution of the Self-Interference

Due to the structure of $\mathbf{A}$, each row i of $\mathbf{S}$ is a permutation of its first row and the ith element of the row is 1 because of the normalized transmit and receive filters. The elements of $\mathbf{S}$ that are not on the diagonal constitute the self-interference:

$$\hat{d}_i = d_i + I_i + \tilde{n}_i, \tag{9}$$

where

$$I_i = \sum_{\substack{j=1 \\ j\neq i}}^{KM} \mathbf{S}_{ij} d_j \qquad \text{and} \qquad \tilde{n}_i = \sum_{j=1}^{KM} \mathbf{A}^*_{ji} n_j \tag{10}$$

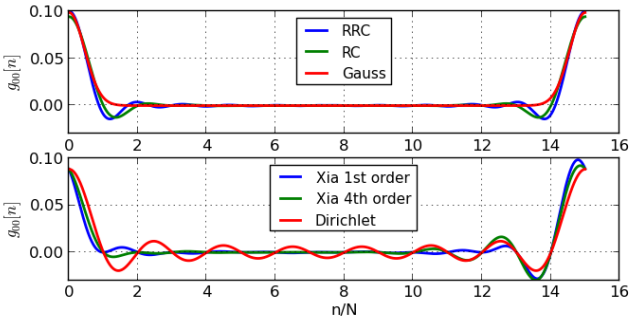

Fig. 2. Time domain responses of the GFDM pulse shaping filters. The rolloff for RC, RRC, and the Xia pulses was set to $\alpha = 0.5$ and for the Gaussian $\alpha = 2$.

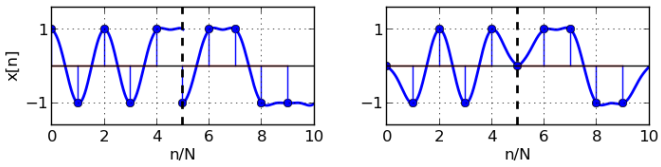

(a) No guard symbol (b) One guard symbol

Fig. 3. Illustration of the guard symbol for two GFDM blocks, $M = 5$. The guard symbol reduces the steep change of the signal between both blocks.

and $(\cdot)^*$ denotes complex conjugation. I_i in (9) describes the self-interference and shall be modeled as a random variable I_i in the following. Its probability density function and variance is given by

$$p(I_i) = \underset{\substack{j=1 \\ j\neq i}}{\overset{KM}{\circledast}} p(\mathbf{S}_{ij} d_j), \tag{11}$$

$$\text{Var}(I_i) = -1 + \sum_{j=1}^{KM} |\mathbf{S}_{ij}|^2. \tag{12}$$

Since the rows of $\mathbf{S}$ are permutations of each other and the d_i are i.i.d. the probability distribution of I_i is independent of the symbol index i. Accordingly I_i will be denoted with I from now on. Under the simplifying assumption of purely real or imaginary $\mathbf{S}_{1j}$, which is the case for the presented pulses, the real and imaginary parts of I are i.i.d. and therefore it suffices to solely analyze the real part. Furthermore when the data symbols are taken from an X-QAM alphabet the probability distribution p_j of $\mathbf{S}_{1j} d_j^R$, where d_j^R is the real part of d_j, is given by

$$p_j(u) = \tfrac{1}{|\mathcal{D}|} \sum_{d\in\mathcal{D}} \delta(u - \mathbf{S}_{1j} d). \tag{13}$$

Here, $\mathcal{D}$ is the set of all possible modulation points on the real axis. It follows that $p(I)$ is a discrete distribution consisting of delta pulses that are located at every possible outcome of $\sum_{j=2}^{KM} \mathbf{S}_{1j} d_j$, where each $d_j \in \mathcal{D}$. Consequently the number of locations of the delta pulses exponentially increases with the modulation order and their density in the interference values has been observed to approach a Gaussian distribution. This is depicted in Fig. 4 where the interference distribution was simulated with a RRC filter and QPSK and 16-QAM. It is clearly shown that the distribution becomes continuous with a higher modulation order. Accordingly, the distribution $p(I)$ can be modeled Gaussian with variance equal to (12) when using 16-QAM or higher order modulations.

B. Closed Form BER Expression

With known interference distribution $p(I)$, the channel noise term in (9) can be reconsidered. By reason of the structure of $\mathbf{A}$ the variance of the noise is equal for every symbol and given by

$$\text{Var}(\tilde{n}) = \sigma_n^2 \sum_{n=0}^{NM-1} |g[n]|^2 = \sigma_n^2 \tag{14}$$

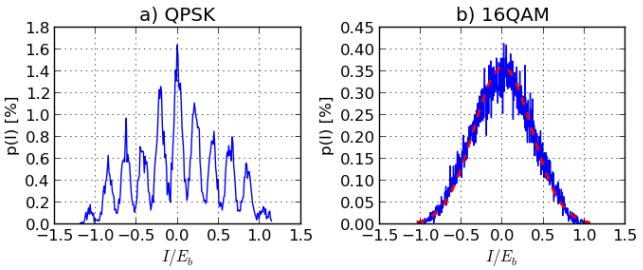

Fig. 4. Interference distribution for QPSK and 16QAM. Used parameters: M=15, K=128, RRC pulse filter with $\alpha = 1$.

and $\tilde{n}$ is still normal distributed where the last equality follows from the normalization of $g[n]$.

For QPSK modulation the discrete interference distribution is considered directly and the resulting BER can be calculated by the law of total probability as

$$P(\text{Bit Error}) = \sum_{k \in \mathcal{I}} P(\text{Bit Error}|I = k)P(I = k) \tag{15}$$

where $\mathcal{I}$ is the set of all possible realizations of I. $P(\text{Bit Error}|I = k)$ can be regarded as the probability of a bit error under the influence of Gaussian noise with variance σ_n^2 and mean $\mu = k$.

Starting from the well-known equation for the BER of QPSK over AWGN which also holds for OFDM

$$P_{\text{OFDM}}(\text{Bit Error}) = Q\left(\sqrt{\frac{2E_b}{N_0}}\right) \tag{16}$$

one can consider the interference terms to result in a closed form expression for the BER of GFDM with QPSK modulation

$$P_{\text{GFDM}}(\text{Bit Error}) = \sum_{k \in \mathcal{I}} P(I = k) Q\left(\sqrt{\frac{2E_b}{N_0}}(1 - k)\right), \tag{17}$$

with $E_b/N_0 = (2\sigma_n^2)^{-1}$. Note that (17) becomes (16) when $p_j(I) = \delta(I)$, i.e. when the system is orthogonal.

For 16-QAM and higher orders the interference term and the channel noise term in (9) are both considered normal distributed and add up to an overall normal distributed noise term with variance $\sigma_o^2 = \text{Var}(I) + \sigma_n^2$ whereas OFDM would only suffer from σ_n^2 as the overall noise variance. The resulting BER is expressed with a generic equation for the BER of X-QAM over AWGN [11]:

$$P_{\text{X-QAM}}(\text{Bit Error}) = \frac{1}{\log_2 \sqrt{X}} \sum_{k=1}^{\log_2 \sqrt{X}} P_b(k), \tag{18}$$

with

$$P_b(k) = \frac{1}{\sqrt{X}} \sum_{i=0}^{(1-2^{-k})\sqrt{X}-1} \left\{ (-1)^{\left\lfloor \frac{i \cdot 2^{k-1}}{\sqrt{X}} \right\rfloor} \times \left(2^{k-1} - \left\lfloor \frac{i \cdot 2^{k-1}}{\sqrt{X}} + \frac{1}{2} \right\rfloor\right) \cdot \text{erfc}\left((2i+1)\sqrt{\frac{3\log_2 X \cdot \gamma}{2(X-1)}}\right)\right\}, \tag{19}$$

where X is the number of modulation symbols and $\gamma = \frac{1}{2\sigma_o^2}$ is the modified SNR due to the self-interference.

IV. Power Spectral Density (PSD) of GFDM

The PSD of a baseband signal is calculated according to [12] by

$$P(f) = \lim_{T \to \infty} \left(\frac{1}{T} E\{|\mathcal{F}\{x_T(t)\}|^2\}\right) \tag{20}$$

where $x_T(t)$ is the transmit signal that is truncated to the interval $(-T/2, T/2)$. In the GFDM case, $x_T(t)$ is the concatenation of multiple GFDM blocks

$$x_T(t) = \sum_{v,m,k} d_{vmk} g_{0m}(t - vMT_s) e^{-j2\pi \frac{k}{T_s} t} \tag{21}$$

$$X_T(f) = \sum_{v,m,k} d_{vmk} G_m(f - \frac{k}{T_s}) e^{-j2\pi v M T_s f} \tag{22}$$

where v is the block index that ranges from $-\frac{T}{2MT_s}$ to $+\frac{T}{2MT_s}$ and $X_T(f)$ and $G_m(f)$ are the Fourier transforms of $x_T(t)$ and $g_{0m}(t)$, respectively. Under the condition of i.i.d. data symbols with unit variance, inserting (22) into (20) yields the PSD of a GFDM system as:

$$P(f) = \frac{1}{MT_s} \sum_{k,m} \left| G_m\left(f - \frac{k}{T_s}\right)\right|^2. \tag{23}$$

V. System Performance

In this section, the GFDM BER and OOB radiation for different pulse shaping filters are compared with a corresponding OFDM system.

TABLE I
Simulation Setup

Parameter	Notation	GFDM	OFDM
Sampling frequency	f_s	1.92 MHz	
Subcarrier spacing	F	15 kHz	
Symbol duration	T_s	66.6 μs	
Subcarrier count	K	128	
Samples per symbol	N	128	
Symbols per block	M	15	1
Pulse shape	g	see Sec. II.D.	rectangular

A. Simulation Setup

The parameters of the GFDM and OFDM system are shown in Tab. I. The OFDM system has been designed with similar parameters to ensure a fair comparison.

Each system is simulated with 128 subcarriers, where the subcarriers 20 through 40 are switched off to investigate the OOB leakage. The OOB leakage is defined to be the ratio between the average energy in the OOB region and the average energy in the allocated subcarriers

$$O = \frac{|\mathcal{B}|}{|\mathcal{OOB}|} \cdot \frac{\int_{f\in\mathcal{OOB}} P(f)df}{\int_{f\in\mathcal{B}} P(f)df}, \tag{24}$$

where $\mathcal{B}$ and $\mathcal{OOB}$ are the set of frequencies that are considered in-band and out of band, respectively. For the present evaluation two measures that employ either 1 or 6 guard carriers between $\mathcal{B}$ and $\mathcal{OOB}$ are investigated. We have chosen 1 guard carrier to show that GFDM fulfills the FCC regulation of 50 dB OOB suppression even with a very high spectral efficiency and 6 guard carriers to show the immense drop rate of the OOB radiation of the GFDM system compared to OFDM. Fig. 5 illustrates the concept of the OOB measurement with guard carriers.

B. Simulation Results

1) OOB Leakage: The PSD of an exemplary comparison between OFDM and GFDM is shown in Fig. 6 and numerical results are given in Tab. II. GFDM is simulated with zero or one guard symbols. Evidently, in this simulation GFDM has an OOB suppression of 11dB or 39 dB higher than OFDM when using zero or one guard symbols and 1 guard carrier, respectively. When using 6 guard carriers the GFDM OOB suppression is even 50 dB higher compared to OFDM when using one guard symbol.

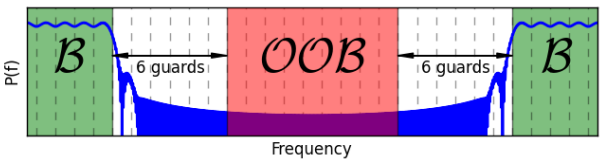

Fig. 5. Illustration of OOB measurement with 6 guard carriers.

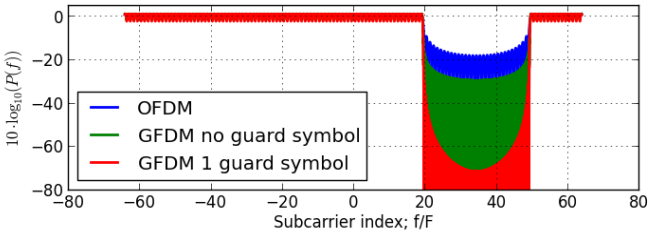

Fig. 6. Spectrum comparison of OFDM and GFDM. GFDM uses a RC filter with rolloff $\alpha = 0.5$. The subcarriers 21 to 50 are switched off.

TABLE II
OOB LEAKAGE IN DB OF THE SIMULATION IN FIG. 6.

Guards	OFDM	GFDM no guard symbol	GFDM 1 guard symbol
1	-19.2	-30.4	-58.3
6	-21.2	-32.4	-71.4

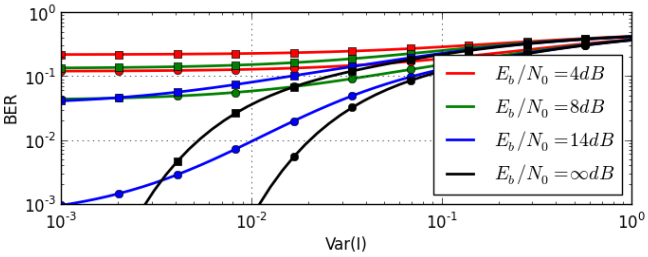

Fig. 7. Resulting BER for different interference values. Circles: 16QAM, Squares: 64QAM.

2) BER performance: The BER of a GFDM system in an AWGN channel is directly connected to $\mathrm{Var}(I)$ of the employed pulse shaping filter. The relationship is shown in Fig. 7 where the BER for a GFDM system depending on the self-interference variance is shown for different noise powers. Naturally, the BER increases with the self-interference variance but only if the self-interference exceeds some critical value that depends on the noise power. This critical value increases with the noise power which means that for low SNR an increased interference does not have a large influence on the BER. On the other hand when the SNR becomes larger even a small change in the variance constitutes a significant change in the BER.

Consequently, when operating in an environment with high SNR a pulse shaping filter with low interference should be preferred in order to achieve a good BER. Conversely in environments with low SNR a pulse shaping filter with higher interference can be used which in turn might have better spectral properties. Simulation results for zero-forcing and linear MMSE receivers in AWGN and Rayleigh-fading channels are provided in [7] but no theoretic equations are derived there.

3) Filter performance: The relation between the interference variance and the OOB leakage with one guard symbol of the investigated pulse shaping filters is shown in Fig. 8. In general, the curves are similar in both diagrams, but naturally the OOB leakage with 6 guard carriers is below that with 1 guard carrier. All of the present pulse shaping filters outperform OFDM regarding the OOB radiation by at least 19dB.

The Gaussian pulse shows the highest variance ($\approx$ 0.2), relatively independent of its α, but it can reach the lowest OOB leakage when accepting 6 guard carriers (-93 dB). The RRC filter has a comparable variance to the RC and Xia pulses but exhibits a stronger OOB radiation ($\approx$ 10 dB higher). This is caused by the abrupt transition between the GFDM blocks when the transmit filter is not ISI-free. When $\alpha = 0$ the RC

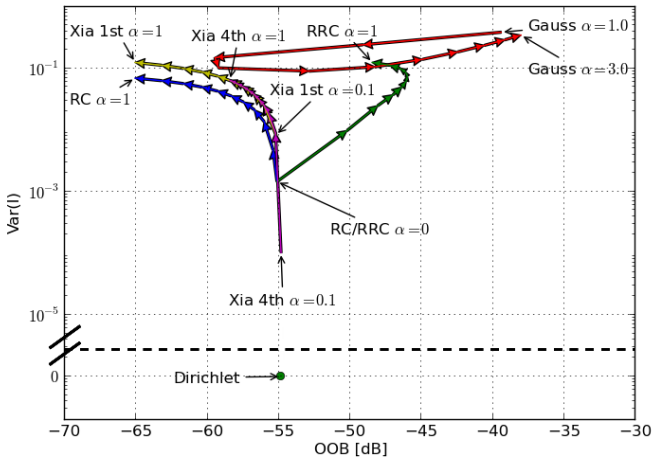

(a) 1 guard carrier

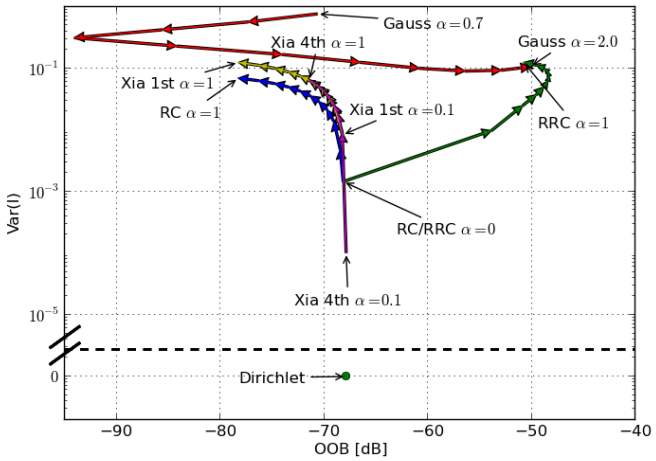

(b) 6 guard carriers

Fig. 8. OOB radiation and interference variance for GFDM with different pulse shaping filters and 1 guard symbol. Note the discontinuity in the y-axis for showing the Dirichlet pulse.

and RRC both simplify to a standard $\mathrm{sinc}(n/N)$ and therefore show the same performance. The RC pulse shows a OOB leakage that is about 40 dB or 50 dB below that of OFDM when inserting 1 or 6 guard carriers, respectively. The 1st order Xia pulse shows an OOB radation equal to that of the RC, but suffers from a larger interference (2 dB). The 4th order pulse suffers from a higher OOB radiation but can reach lower interference variances than the RC. Finally, the Dirichlet pulse shaping filter creates no self-interference at all but has a OOB radiation comparable to the RC with $\alpha = 0$ (-68 dB with 6 guard carriers). Hence, the Dirichlet pulse makes the GFDM system orthogonal and reach the same BER as OFDM in an AWGN channel, where at the same time the OOB radiation is suppressed to 46 dB below OFDM. GFDM with a Dirichlet pulse can therefore be regarded as a "reversed OFDM" where the rect pulse shaping is applied in the frequency domain instead of the time domain. However, with the Dirichlet filter a larger sensitivity to timing-offsets may arise.

VI. Conclusion

GFDM is a block-based multicarrier scheme that employs pulse shaping per subcarrier to reduce its OOB radiation whereupon self-interference can appear. Closed form expressions for the PSD and the BER of GFDM with a matched filter receiver were derived and used to evaluate the performance of different pulse shaping filters. It was shown that filters that are ISI-free after transmission create a significantly lower OOB radiation when using 1 guard symbol in each GFDM block. In the presented simulations GFDM is able to reduce the OOB radiation to an amount of roughly 48dB below that of OFDM when measuring with 6 guard carriers. The RC pulse shaping filter was found to have an acceptable interference while at the same time it offers the possibility to reduce the OOB radiation down to 58 dB below OFDM. The Dirichlet pulse makes the GFDM system orthogonal and it can reach the same BER as OFDM in an AWGN channel.

Acknowledgment

This work has been performed in the framework of the ICT project ICT-318555 "5GNOW", which is partly funded by the European Union.

References

[1] T. Ihalainen, A. Viholainen, T. H. Stitz, and M. Renfors, "Generation of Filter Bank-Based Multicarrier Waveform Using Partial Synthesis and Time Domain Interpolation," *IEEE Transactions on Circuits and Systems I: Regular Papers*, vol. 57, no. 7, pp. 1767–1778, Jul. 2010.

[2] G. Fettweis, M. Krondorf, and S. Bittner, "GFDM - Generalized Frequency Division Multiplexing," in *VTC Spring 2009 - IEEE 69th Vehicular Technology Conference*. IEEE, Apr. 2009, pp. 1–4.

[3] P. Siohan, C. Siclet, and N. Lacaille, "Analysis and design of OFDM/OQAM systems based on filterbank theory," *Signal Processing, IEEE Transactions on*, vol. 50, no. 5, pp. 1170–1183, May 2002.

[4] A. Viholainen, T. Ihalainen, T. H. Stitz, M. Renfors, and M. Bellanger, "Prototype filter design for filter bank based multicarrier transmission," in *Proceedings of European Signal Processing Conference (EUSIPCO)*, 2009.

[5] R. W. Chang, "Synthesis of Band-Limited Orthogonal Signals for Multichannel Data Transmission," *The Bell Systems Technical Journal*, vol. 45, no. 10, pp. 1775–1796, 1966.

[6] R. Datta, N. Michailow, M. Lentmaier, and G. Fettweis, "GFDM Interference Cancellation for Flexible Cognitive Radio PHY Design," in *2012 IEEE Vehicular Technology Conference (VTC Fall)*. IEEE, Sep. 2012, pp. 1–5.

[7] N. Michailow, S. Krone, M. Lentmaier, and G. Fettweis, "Bit Error Rate Performance of Generalized Frequency Division Multiplexing," in *2012 IEEE Vehicular Technology Conference (VTC Fall)*. IEEE, Sep. 2012, pp. 1–5.

[8] X. Xia, "A family of pulse-shaping filters with ISI-free matched and unmatched filter properties," *Communications, IEEE Transactions on*, vol. 45, no. 10, pp. 1157–1158, 1997.

[9] C. C. Tan and N. C. Beaulieu, "An investigation of transmission properties of Xia pulses," in *Communications, 1999. ICC '99. 1999 IEEE International Conference on*, vol. 2, 1999, pp. 1197–1201 vol.2.

[10] A. M. Bruckner, J. B. Bruckner, and B. S. Thomson, *Real analysis*. Prentice Hall PTR ISBN: 9780134588865, 1997.

[11] K. Cho and D. Yoon, "On the general BER expression of one- and two-dimensional amplitude modulations," *IEEE Transactions on Communications*, vol. 50, no. 7, pp. 1074–1080, Jul. 2002.

[12] T. van Waterschoot, V. Le Nir, J. Duplicy, and M. Moonen, "Analytical Expressions for the Power Spectral Density of CP-OFDM and ZP-OFDM Signals," *Signal Processing Letters, IEEE*, vol. 17, no. 4, pp. 371–374, Apr. 2010.